Influence of surface passivation on the electrical properties of p–i–n GaAsP nanowires

O. Saket, C. Himwas, A. Cattoni, F. Oehler, F. Bayle, S. Collin, L. Travers, A. Babichev, F. H Julien, J. C Harmand, et al.

Applied Physics Letters

Influence of surface passivation on the electrical properties of p–i–n GaAsP nanowires

Cite as: Appl. Phys. Lett. **117**, 123104 (2020); https://doi.org/10.1063/5.0022157
Submitted: 17 July 2020 . Accepted: 03 September 2020 . Published Online: 22 September 2020

O. Saket, C. Himwas, A. Cattoni, F. Oehler, F. Bayle, S. Collin, L. Travers, A. Babichev, F. H. Julien, J. C. Harmand, and M. Tchernycheva

Applied Physics Letters ARTICLE scitation.org/journal/apl

Influence of surface passivation on the electrical properties of p–i–n GaAsP nanowires

Cite as: Appl. Phys. Lett. **117**, 123104 (2020); doi: 10.1063/5.0022157
Submitted: 17 July 2020 · Accepted: 3 September 2020 ·
Published Online: 22 September 2020

O. Saket,[1] C. Himwas,[2] A. Cattoni,[1] F. Oehler,[1] F. Bayle,[1] S. Collin,[1] L. Travers,[1] A. Babichev,[3] F. H. Julien,[1] J. C. Harmand,[1] and M. Tchernycheva[1,a)]

AFFILIATIONS

[1]Centre de Nanosciences et de Nanotechnologies (C2N), UMR 9001 CNRS, University Paris Sud, University Paris-Saclay, 8 Avenue de la Vauve, 91120 Palaiseau, France
[2]Chulalongkorn University, Semiconductor Device Research Laboratory, Department of Electrical Engineering, Faculty of Engineering, 254 Phayathai Road, 10330 Bangkok, Thailand
[3]ITMO University, 49 Kronverksky Pr., 197101 St. Petersburg, Russia

[a)]**Author to whom correspondence should be addressed:** maria.tchernycheva@u-psud.fr

ABSTRACT

The electrical properties of passivated and non-passivated axial p–i–n junctions in GaAsP nanowires are investigated using electron-beam induced current microscopy. Organized self-catalyzed p–i–n nanowires having different segment lengths are grown by molecular-beam epitaxy on nanopatterned Si substrates. The nanowires are *in situ* passivated with a GaP shell. The position of the junction is found to be dependent on the length of the upper Be-doped segment evidencing the diffusion of Be atoms from the upper segment to the bottom part of the nanowire. Comparison between non-passivated and passivated nanowires shows a strong enhancement of the collection region after passivation. The results also prove the existence of a p-doped shell around the nanowires formed due to a parasitic radial growth. This shell is depleted in non-passivated nanowires; however, it becomes electrically active after surface passivation modifying the carrier collection pattern.

Today, single bandgap solar cells start to approach the Shockley–Queisser limit[1] with a record of efficiency of 29.1% for GaAs and 27.6% for Si devices.[2] To go beyond this limit, a multiple junction architecture instead of single bandgap cells can be used. The record is given by a four-junction solar cell demonstrating a 47.1% conversion efficiency.[2] However, the wide spread of multi-bandgap devices is still limited by the high cost of III–V materials and the difficulty to deal with the lattice mismatch between different layers in a stack. Recently, III–V semiconductor nanowires (NWs) have emerged as a good alternative for thin-film solar cells.[3–10] NWs are elongated nanocrystals characterized by a small diameter (around 100 nm) and a length of a few micrometers. Their nanoscale footprint and the free lateral surface allow NWs to relax strain and they can be grown on lattice-mismatched substrates without dislocations.[11,12] In the past few years, NW solar cells have made fast progress, and to date, they have reached 15.3% of efficiency for GaAs[13] and 15% for InP[14] bottom-up NWs and 17.8% on top-down approach.[15] Tandem III–V NW/Si solar cells have been theoretically proposed showing that the optimal bandgap for the III–V subcell is around 1.7 eV.[16] Experimentally, NW/Si tandem devices have been demonstrated; however, their performance is well below the single bandgap NW cell record.[17,18]

One serious candidate for the top cell material in III–V/Si tandem devices is GaAsP. Several investigations of GaAsP NWs have been reported;[10,19–24] however, the efficiency of GaAsP NW solar cells remains low. This is due to a more complex control over the optical and electrical properties of a ternary alloy and to a lack of knowledge of several fundamental parameters. In particular, the surface passivation of GaAsP NWs has not been sufficiently studied, while it is one of those strongly affected by the surface effects. Surface states modify the electronic band structure and the intrinsic properties of the NWs[25,26] and lead to increased non-radiative recombinations degrading the carrier collection. The surface recombination can be strongly reduced by either *ex situ* or *in situ* NW passivation. In the literature, analyses of the surface passivation mainly focus on the NW optical properties[19,22,23] with only a few assessments of the electrical properties.[14,21,27,28] In particular, there is only one report on the impact of passivation on the electrical properties of GaAsP NW solar cells; however, it is done for a

core/shell architecture, while the passivation of axial junction GaAsP NWs remains unexplored.

In this Letter, we analyze the electrical properties of bare and passivated $GaAs_{0.7}P_{0.3}$ NWs containing different axial p–i–n junctions. Organized arrays of self-catalyzed GaAsP NWs are grown by molecular-beam epitaxy (MBE) on nanopatterned Si (111) substrates using Be and Si as doping sources. The surface passivation is performed by the *in situ* growth of GaP shell around the NWs. Electron-beam induced current (EBIC) microscopy is used to investigate the electrical activity of passivated and non-passivated individual NWs. First, EBIC microscopy is applied to GaAsP non-passivated NWs containing axial p–i–n junction with different lengths of the p-doped upper part. The position of the junctions is found to be dependent on the length of the p-type segment evidencing a residual n-type doping of the GaAsP intrinsic segment and also the diffusion of Be atom from the upper segment to the bottom part of the NWs. The results prove the existence of a p-doped shell around the NWs formed by the parasitic radial growth during the deposition of the Be-doped segment. Next, EBIC maps of bare and passivated NWs with an identical structure of the core are compared showing a strong broadening of the collection region after passivation. The analyses of the EBIC profiles prove the existence of a spontaneously formed p-doped shell around the NWs formed during the growth of the upper Be-doped segment. This shell is depleted in non-passivated NWs, while it becomes electrically active after surface passivation, thus modifying the carrier collection pattern.

The GaAsP NWs were grown on patterned n-type Si (111) substrates by MBE following the previously optimized procedure.[24,29] Hexagonal arrays of nano-holes in a SiO_2 mask layer were defined by electron-beam lithography. The patterned substrates were outgassed in an ultra-high vacuum chamber at 450 °C for one hour prior to the NW growth. NWs were grown at 610 °C by a vapor–liquid–solid mechanism in a self-catalyzed growth mode. First, a short deposition of gallium (Ga) was performed in order to form Ga droplets in the nano-holes. Then, the Arsenic (As) and Phosphorus (P) shutters were opened simultaneously to initiate the growth of GaAsP NWs. The Ga flux was adjusted to be equivalent to a 2D growth rate on GaAs (001) of 0.2 nm·s^{-1}. As and P were supplied by solid-source cells in the form of As_4 and P_2. The V-to-III beam equivalent pressure (BEP) ratio was set equal to 9, while the $P_2/(P_2+As_4)$ BEP ratio was adjusted to 0.2. Axial p–i–n junctions were obtained by opening and closing the doping cell shutters during the GaAsP NW growths. Be and Si were used to dope the NWs, respectively, p- and n-types, as previously demonstrated in Ref. 6. The temperature of the Si (Be) cell was set to 1150 °C (700 °C). According to the EBIC measurements, these temperatures were shown to yield an NW doping concentration of around $7 \pm 4 \times 10^{17}$ cm^{-3} and $9 \pm 5 \times 10^{17}$ cm^{-3} for electrons and holes, respectively. The alloy composition was probed by energy-dispersive x-ray spectroscopy (EDX) showing a homogeneous P concentration along the wire axis close to 28%,[22] which corresponds to the optimal bandgap for III-V NW on Si tandem devices. Figure 1(a) shows a representative SEM image of an organized GaAsP NW array containing p–i–n junctions.

Three p–i–n samples with different segment lengths were elaborated. The length of the corresponding segments was adjusted by setting the growth time. Sample S1 was grown with the same deposition time of 8 min for the p-, i-, and n- segments. In sample S2, the growth time for each segment was reduced to 6 min. Sample S3 has the same total deposition time as sample S2; however, the n-doped segment was deposited during 10 min, the undoped segment was deposited for 6 min, while the deposition time of the p-doped segment was reduced to 2 min. Table I summarizes the growth time of the three segments of the p–i–n junctions for all the samples.

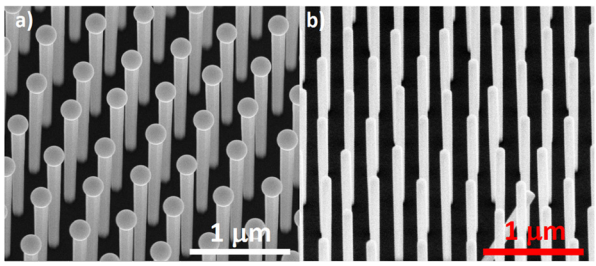

FIG. 1. (a) 25° tilted SEM image of GaAsP NW array containing axials p–i–n junctions; (b) 45° tilted SEM image of the GaAsP NW array after passivation with a GaP shell.

Samples $S1^P$ and $S3^P$ with a passivating high bandgap shell around the p–i–n junction were grown for comparison. Sample $S1^P$ ($S3^P$) has an identical structure of the core as S1 (S3), except for a GaP shell. We have previously developed GaP passivation for undoped GaAsP NWs, which was shown to yield a two order of magnitude enhancement of the photoluminescence intensity and carrier lifetime.[22] In the present study, this passivation procedure is applied to active p–i–n junctions. To grow the shell, the Ga droplets were crystallized under element V flux in the presence of Be doping and then the GaAsP NW cores were *in situ* surrounded with an undoped 5-nm-thick GaP shell at a substrate temperature of ∼500 °C.[22,23] The absence of the catalyst and the low substrate temperature favor the NW lateral expansion by the vapor–solid growth.[30,31] The GaP shell growth was performed by opening the Ga and P shutters simultaneously, at the same Ga flux and V-to-III ratio as used for the NW core, for 2 min. Figure 1(b) shows a representative SEM image of an NW array after passivation.

Bare and passivated NWs were analyzed using EBIC microscopy, which is a powerful tool to probe the electrical properties of NWs.[32–34] In this study, we used an SEM Hitachi SU8000 microscope combined with a Kleindiek probe station equipped with 4 tungsten tips to directly contact individual NWs. The induced current is amplified with an SR570 current preamplifier, and a Gatan Digscan system is used to construct the EBIC map point by point. For each scan, the morphological SEM image and the corresponding induced current

TABLE I. Growth sequence for the analyzed GaAsP p–i–n samples. All values refer to the growth time in min.

Sample\Growth time, min	GaAsP n-type	GaAsP undoped	GaAsP p-type	GaP shell
S1	8	8	8	No shell
S2	6	6	6	No shell
S3	10	6	2	No shell
$S1^P$	8	8	8	2
$S3^P$	10	6	2	2

map are recorded simultaneously. All measurements are performed at a 7 kV acceleration voltage and an injected current of ∼55 pA. All EBIC profiles are based on a regular mesh with a 6 nm distance between the neighboring points To reduce the noise, all line profiles are averaged over a 20 nm wide region in the direction normal to the wire axis.

EBIC microscopy was first applied to the bare p–i–n NWs to probe the effective doping profile. Figures 2(a)–2(c) displays the NW schematic, the SEM image, and the EBIC map without the external bias of representative NWs from samples S1, S2, and S3, respectively. The corresponding EBIC profiles along the wire axis are reported in [Figs. 2(d)–2(f)]. The nominal position of the three doping segments composing the junction (p, i, and n) are indicated by assuming that the growth rate is constant in time and is independent of the doping type.

One important observation from the comparison of the EBIC maps for S1, S2, and S3 is that the collection region in these NWs is located at different positions. We observe that for S3, which has the shortest p-doped segment, the collection region is localized at the top of the undoped segment close to the i-/p- interface [Fig. 2(c)]. This is not consistent with the nominal p–i–n structure of the NWs, which should result in a wide collection region overlapping with the i-segment. The localized collection peaked at the i-/p-interface indicates the presence of a residual n-type doping in the intrinsic region, which transforms the nominal p–i–n junction into a p–n–n structure. Indeed, it was reported in the literature that intrinsic GaAs NWs are residually n-type doped for the NW diameters $d > 70$ nm.[35] Given that the diameter of our NWs is around 90 ± 10 nm, our results for GaAsP NWs are consistent with a residual n-type doping similar to the case of GaAs NWs.[35] When the length of the Be-doped segment is increased in sample S2 and further in sample S1, the collection region moves down: it is located in the i-segment for S2 and it is in the n-doped segment close to the i-/n-interface in S1.

One possible explanation for this observation may be the diffusion of Be atoms during the growth of the top p-doped segment into the intrinsic region of the NW, as has been previously reported.[36] Both axial from the top segment and radial diffusions from the sidewalls are possible. This diffusion progressively compensates the residual n-type doping of the nominally undoped segment. Therefore, the collection region is shifted to be in the middle of the i-segment [Fig. 2(b)] for S2.

We note that the effective doping profile of the intrinsic segment probably depends on the position, so that it has a propensity to be p-doped at the top and n-doped at the bottom.

For S1, the induced current presents its maximum in the n-type segment ∼150–200 nm below the i-/n- interface, which indicates a partial compensation of the intentional n-type doping of the bottom segment. Second electron (SE) contrast, which is sensitive to the doping type, also confirms this hypothesis [Fig. 2(a)]. However, we note that the estimated position of the n-/i-interface may not be exact since we assume that the NW growth starts immediately after opening the P and As shutters. As we do not account for any NW incubation time (growth delay) or transient axial growth rate at the early stage of growth,[29] the length of the first n-doped segment may be slightly overestimated. Due to the Be diffusion, the effective structure for the S1 sample is transformed into a p–p–n junction.

By analyzing the EBIC profiles illustrated in [Figs. 2(d)–2(f)], we observe that the width W of the collection region also varies from sample S1 to S3: for S1, $W = 100 \pm 20$ nm, for S2, it increases to

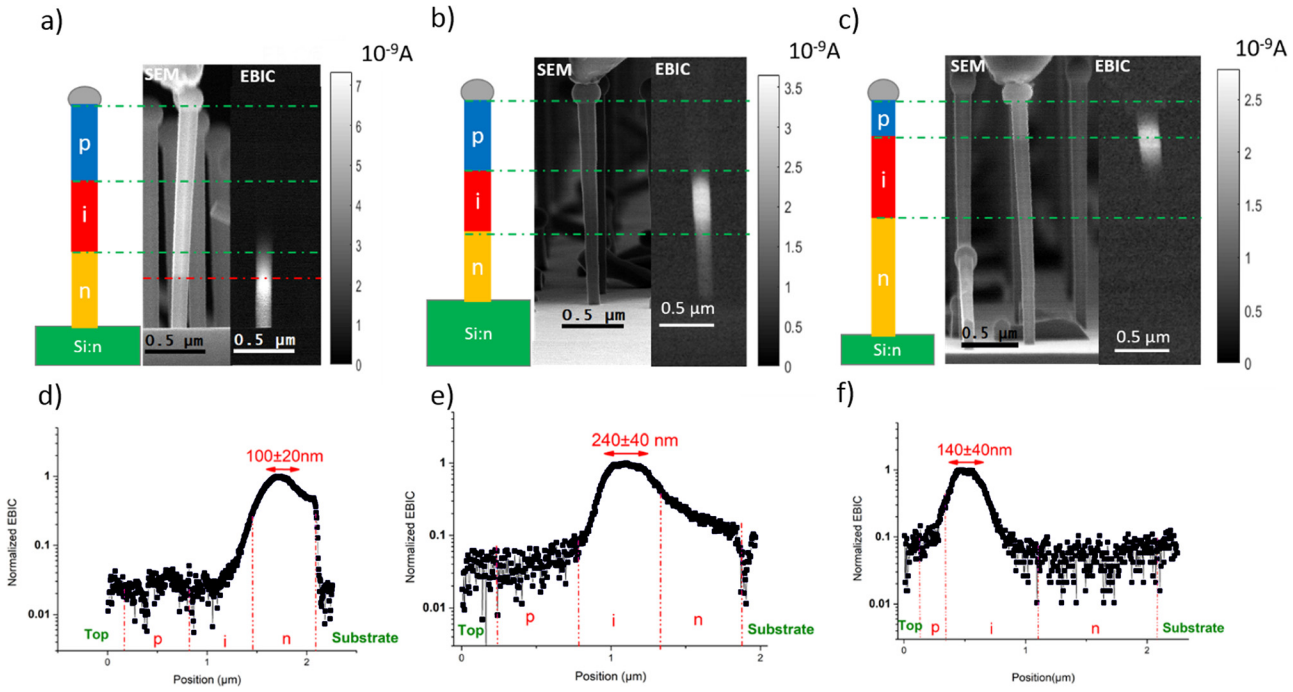

FIG. 2. (a) Schematic, SEM image and the corresponding EBIC map of a single NW from sample S1, (b) same for S2, (c) same for S3, (d) normalized EBIC profile corresponding to the EBIC map in panel (a), (e) same for panel (b), and (f) same for panel (c). The dashed lines in panels (d)–(f) indicate the nominal positions of the p-, i-, and n-doped segments, respectively.

W = 240 ± 40 nm, and for S3, it again decreases to W = 140 ± 40 nm. This small depletion region width in S1 and S3 is consistent with the effective doping of p–p–n for S1 and p–n–n for S3. For the S2 sample, the depletion region is broadened, which indicates that the effective structure is closer to the nominal p–i–n one.

To probe the effect of surface passivation on the electrical properties of these NWs, EBIC analyses were performed on the passivated p–i–n junctions $S1^P$ and $S3^P$, as illustrated in [Figs. 3(a) and 3(d)]. Contrary to bare p–i–n junctions, the maps of passivated NWs show a wide collection region. Figures 3(b) and 3(e) compares in the same graph the EBIC profiles of the NWs having the same core structure and differing only by the passivating shell. The collection region is strongly extended by the surface passivation increasing from 0.1 μm in S1 to 0.76 μm in $S1^P$ (from 0.14 μm in S3 to 1.45 μm in $S3^P$). By fitting the current decay in the left part of the profiles, we found that the electron diffusion length in the p-doped segment is increased from 133 ± 10 nm for S1 to 235 ± 10 nm for $S1^P$ and from 95 ± 10 nm for S3 to 223 ± 10 nm for $S3^P$. (We note that the current decrease in passivated samples does not exactly follow the exponential law, so these values remain estimative; however, the increase in the electron diffusion length by a factor of 2 ± 0.5 is observed in all analyzed NWs of the $S1^P$ and $S3^P$ samples (about 10 per sample). From the optical analyses of GaP passivation,[22] a stronger enhancement of the minority carrier diffusion lengths could have been expected. The fact that the electron diffusion length increases with passivation by only a factor of 2 (to be compared with a two order of magnitude enhancement of the photoluminescent intensity in undoped wires[22]) points to the presence of other phenomena limiting the minority carrier diffusion length in addition to the surface recombination. These may be the volume non-radiative recombination due to the high concentration of doping impurities, as well as the presence of stacking faults limiting the carrier diffusion.

It should be noted that the EBIC profiles in samples $S1^P$ and $S3^P$ present a region with a constant induced current extending down to the substrate, which totally covers the n-doped segment in $S1^P$ and both the n-doped and the intrinsic segments in $S3^P$. This constant profile shape is not expected in axial p–i–n junctions. Indeed, according to our EBIC profile simulations described in the supplementary material, the induced current should decrease away from the junction following the shape shown in (Fig. S1) with a characteristic length given by the minority carrier diffusion length. A slowly varying induced current along the wire axis can be obtained in axial p–i–n junctions only for very long minority carrier diffusion lengths, which is not consistent with the EBIC drop toward the NW top evidencing rather short diffusion lengths. On the contrary, this profile shape is typical for NWs having a radial p–n junction instead of the axial one: indeed, core/shell NW solar cells are characterized by a constant EBIC signal along the wire axis.[37] Therefore, the observed EBIC profiles can be explained by the presence of a p-doped shell around the base part of the NW. Following this hypothesis, the effective doping structure of the passivated NWs is schematized in [Figs. 3(c) and 3(f)]. For the

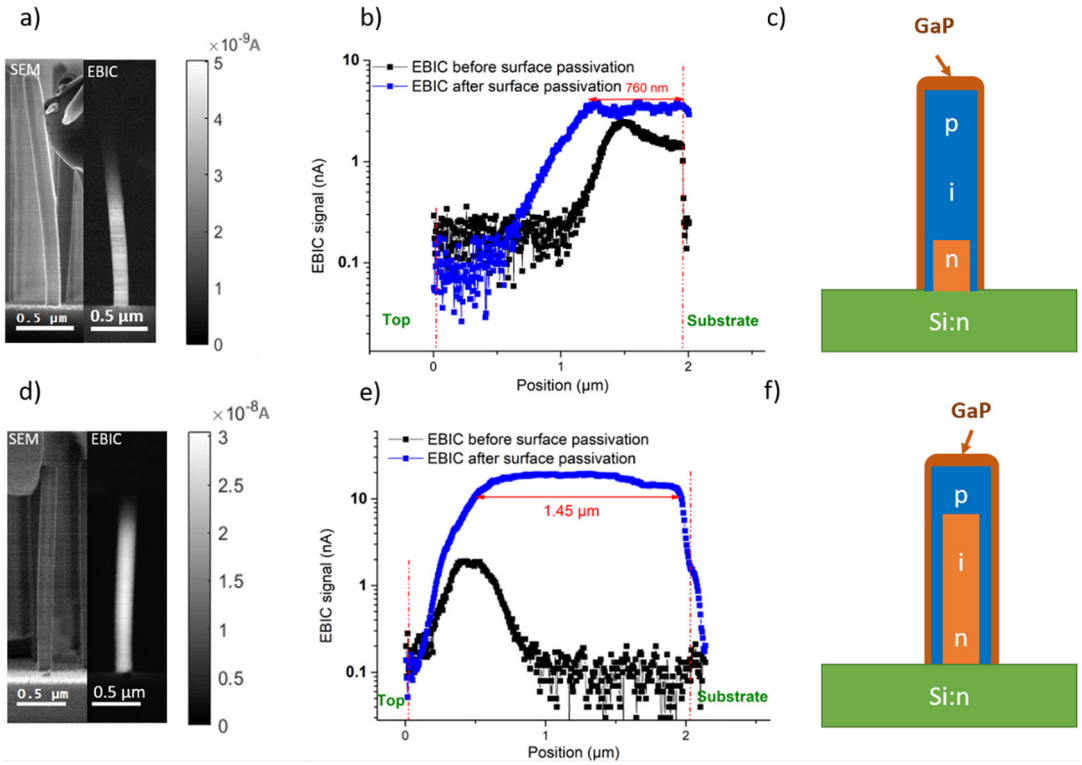

FIG. 3. (a) SEM image of a representative GaAsP NW from sample S1p and the corresponding EBIC map, (b) EBIC profiles along the NW axis for S1 and $S1^P$, (c) schematic of the passivated NWs from sample $S1^P$, (d) same as panel (a) for sample $S3^P$, (e) EBIC profile along the NW axis for S3 and $S3^P$, and (f) schematic of the passivated NWs from sample $S3^P$.

upper part, the carriers are collected by the axial junction, whereas for the lower part, radial separation and collection via the p-doped shell become possible, leading to a flat EBIC profile down to the substrate.

To understand this discrepancy with the nominal structure, it should be reminded that in MBE-grown NWs, a non-intentional shell can be formed around the base part. Indeed, structural and optical characterizations on undoped GaAsP NWs grown under similar conditions showed the formation of an unintentional GaAsP shell due to a parasitic lateral growth by the vapor–solid mechanism, which accompanies the axial NW growth.[23,24] This shell was shown to be optically inactive in bare NWs, but it produced luminescence in NWs passivated with a GaP shell.[23] In the present case of the p–i–n junction NWs, the unintentional shell formed around the base part during the deposition of the top p-doped segment is expected to be p-doped. In addition to the vapor–solid unintentional growth, a p-doped shell can also be formed by the in-diffusion of the Be atoms impinging the NW sidewalls during the p-doped segment growth. In the case of a bare p–i–n junction NW, this unintentional p-doped shell is depleted due to the surface Fermi level pinning, so it does not affect the EBIC profile. However, when the surface is passivated with a GaP deposition, the electrical activity of the unintentional p-doped shell is revealed. The NWs start to behave like a mixed axial and radial junction, thus deviating from their nominal structure. The unintentional p-doped shell induces a radial carrier separation and creates a conducting channel close to the surface, which can transport the photogenerated holes toward the contact.

We note that the shape of the EBIC signal in samples $S1^P$ and $S3^P$ is consistent with our previous conclusions regarding the residual doping of the intrinsic segment: the intrinsic segment exhibits a residual p-type doping in sample $S3^P$, while it behaves as n-doped in sample $S1^P$.

In conclusion, axial passivated and non-passivated GaAsP p–i–n junctions have been elaborated and analyzed by EBIC microscopy. The intrinsic GaAsP segment is found to naturally present a residual n-type doping. The dependence of the junction position in the structure on the length of the upper Be doped segment points to the diffusion of Be atoms in the NWs.

Depending on the growth time of the Be-doped segment, this diffusion can compensate the unintentional doping and revert it to become p-type. Surface passivation strongly increases the collection region. The analysis of the EBIC profiles evidences a mixed axial and radial behavior in passivated NWs, which is attributed to the presence of a Be-doped shell around the NW. This parasitic shell becomes electrically active after surface passivation.

See the supplementary material for details on the simulation of the impact of the surface recombination on the EBIC profile.

This work was financially supported by EU H2020 ERC Project "NanoHarvest" (Grant No. 639052).

DATA AVAILABILITY

The data that support the findings of this study are available from the corresponding author upon reasonable request.

REFERENCES

[1]W. Shockley and H. J. Queisser, J. Appl. Phys. **32**, 510 (1961).
[2]M. A. Green, E. D. Dunlop, J. Hohl-Ebinger, M. Yoshita, N. Kopidakis, and A. W. Y. Ho-Baillie, Prog. Photovoltaics **28**, 3 (2020).
[3]I.-J. Chen, S. Limpert, W. Metaferia, C. Thelander, L. Samuelson, F. Capasso, A. M. Burke, and H. Linke, Nano Lett. **20**, 4064 (2020).
[4]P. Espinet-Gonzalez, E. Barrigon, Y. Chen, G. Otnes, G. Vescovi, C. Mann, J. V. Lloyd, D. Walker, M. D. Kelzenberg, I. Aberg, M. Borgstrom, L. Samuelson, and H. A. Atwater, IEEE J. Photovoltaics **10**, 502 (2020).
[5]V. Raj, L. Fu, H. H. Tan, and C. Jagadish, IEEE J. Photovoltaics **9**, 980 (2019).
[6]O. Saket, C. Himwas, V. Piazza, F. Bayle, A. Cattoni, F. Oehler, G. Patriarche, L. Travers, S. Collin, F. H. Julien, J.-C. Harmand, and M. Tchernycheva, Nanotechnology **31**, 145708 (2020).
[7]M. Vettori, V. Piazza, A. Cattoni, A. Scaccabarozzi, G. Patriarche, P. Regreny, N. Chauvin, C. Botella, G. Grenet, J. Penuelas, A. Fave, M. Tchernycheva, and M. Gendry, Nanotechnology **30**, 084005 (2019).
[8]J. E. M. Haverkort, E. C. Garnett, and E. P. A. M. Bakkers, Appl. Phys. Rev. **5**, 031106 (2018).
[9]D. Mikulik, M. Mintairov, I. Nachemson, V. Evstropov, P. Romero-Gomez, M. Shvarts, and A. Fontcuberta i Morral, Nanotechnology **30**, 094001 (2019).
[10]Y. Zhang, A. M. Sanchez, M. Aagesen, S. Huo, H. A. Fonseka, J. A. Gott, D. Kim, X. Yu, X. Chen, J. Xu, T. Li, H. Zeng, G. Boras, and H. Liu, Small **15**, 1803684 (2018).
[11]F. Glas, Phys. Rev. B **74**, 121302 (2006).
[12]S. Lee, A. Vaid, J. Im, B. Kim, A. Prakash, J. Guénolé, D. Kiener, E. Bitzek, and S. H. Oh, Nat. Commun. **11**, 2367 (2020).
[13]I. Aberg, G. Vescovi, D. Asoli, U. Naseem, J. P. Gilboy, C. Sundvall, A. Dahlgren, K. E. Svensson, N. Anttu, M. T. Bjork, and L. Samuelson, IEEE J. Photovoltaics **6**, 185 (2016).
[14]G. Otnes, E. Barrigón, C. Sundvall, K. E. Svensson, M. Heurlin, G. Siefer, L. Samuelson, I. Åberg, and M. T. Borgström, Nano Lett. **18**, 3038 (2018).
[15]D. van Dam, N. J. J. van Hoof, Y. Cui, P. J. van Veldhoven, E. P. A. M. Bakkers, J. Gómez Rivas, and J. E. M. Haverkort, ACS Nano **10**, 11414 (2016).
[16]R. R. LaPierre, J. Appl. Phys. **110**, 014310 (2011).
[17]M. Yao, S. Cong, S. Arab, N. Huang, M. L. Povinelli, S. B. Cronin, P. D. Dapkus, and C. Zhou, Nano Lett. **15**, 7217 (2015).
[18]B. A. Wood, P. Kuyanov, M. Aagesen, and R. R. LaPierre, J. Photonics Energy **7**, 1 (2017).
[19]Y. Zhang, J. Wu, M. Aagesen, J. Holm, S. Hatch, M. Tang, S. Huo, and H. Liu, Nano Lett. **14**, 4542 (2014).
[20]M. Tchernycheva, L. Rigutti, G. Jacopin, A. de Luna Bugallo, P. Lavenus, F. H. Julien, M. Timofeeva, A. D. Bouravleuv, G. E. Cirlin, V. Dhaka, H. Lipsanen, and L. Largeau, Nanotechnology **23**, 265402 (2012).
[21]J. V. Holm, H. I. Jørgensen, P. Krogstrup, J. Nygård, H. Liu, and M. Aagesen, Nat. Commun. **4**, 1498 (2013).
[22]C. Himwas, S. Collin, P. Rale, N. Chauvin, G. Patriarche, F. Oehler, F. H. Julien, L. Travers, J.-C. Harmand, and M. Tchernycheva, Nanotechnology **28**, 495707 (2017).
[23]C. Himwas, S. Collin, H.-L. Chen, G. Patriarche, F. Oehler, L. Travers, O. Saket, F. H. Julien, J.-C. Harmand, and M. Tchernycheva, Nanotechnology **30**, 304001 (2019).
[24]R. d-e Lépinau, A. Scaccabarozzi, G. Patriarche, L. Travers, S. Collin, A. Cattoni, and F. Oehler, Nanotechnology **30**, 294003 (2019).
[25]M. Speckbacher, J. Treu, T. J. Whittles, W. M. Linhart, X. Xu, K. Saller, V. R. Dhanak, G. Abstreiter, J. J. Finley, T. D. Veal, and G. Koblmüller, Nano Lett. **16**, 5135 (2016).
[26]S. Cuesta, M. Spies, V. Boureau, F. Donatini, M. Hocevar, M. I. den Hertog, and E. Monroy, Nano Lett. **19**, 5506 (2019).
[27]Y. Rui, T. Zhang, D. Zhu, Y. Feng, A. N. Cartwright, M. T. Swihart, Y. Yang, T. Zhang, C. Huang, H. Wang, and D. Gu, J. Phys. Chem. C **123**, 4664 (2019).
[28]A. D. Mallorquí, E. Alarcón-Lladó, I. C. Mundet, A. Kiani, B. Demaurex, S. De Wolf, A. Menzel, M. Zacharias, and A. Fontcuberta i Morral, Nano Res. **8**, 673–681 (2015).
[29]F. Oehler, A. Cattoni, A. Scaccabarozzi, G. Patriarche, F. Glas, and J.-C. Harmand, Nano Lett. **18**, 701 (2018).

[30]S. Morkötter, N. Jeon, D. Rudolph, B. Loitsch, D. Spirkoska, E. Hoffmann, M. Döblinger, S. Matich, J. J. Finley, L. J. Lauhon, G. Abstreiter, and G. Koblmüller, Nano Lett. **15**, 3295 (2015).
[31]C. Colombo, M. Heiβ, M. Grätzel, and A. Fontcuberta i Morral, Appl. Phys. Lett. **94**, 173108 (2009).
[32]H. J. Leamy, J. Appl. Phys. **53**, R51 (1982).
[33]C. Donolato, Phys. Status Solidi A **65**, 649 (1981).
[34]L. Pasemann, Ultramicroscopy **6**, 237 (1981).
[35]N. Han, F. Wang, J. J. Hou, F. Xiu, S. Yip, A. T. Hui, T. Hung, and J. C. Ho, ACS Nano **6**, 4428 (2012).
[36]A. Casadei, P. Krogstrup, M. Heiss, J. A. Röhr, C. Colombo, T. Ruelle, S. Upadhyay, C. B. Sørensen, J. Nygård, and A. Fontcuberta i Morral, Appl. Phys. Lett. **102**, 013117 (2013).
[37]V. Piazza, M. Vettori, A. A. Ahmed, P. Lavenus, F. Bayle, N. Chauvin, F. H. Julien, P. Regreny, G. Patriarche, A. Fave, M. Gendry, and M. Tchernycheva, Nanoscale **10**, 20207 (2018).